THE JOURNAL OF PHYSICAL CHEMISTRY C

Article

Cite This: J. Phys. Chem. C 2018, 122, 14805−14813

pubs.acs.org/JPCC

Polarization-Controlled Directional Multiphoton Photoemission from Hot Spots on Single Au Nanoshells

Jacob Pettine,[†,‡] Andrej Grubisic,[∥] and David J. Nesbitt*[,†,‡,§]

[†]JILA, University of Colorado Boulder and National Institute of Standard and Technology, Boulder, Colorado 80309, United States

[‡]Department of Physics and [§]Department of Chemistry and Biochemistry, University of Colorado Boulder, Boulder, Colorado 80309, United States

[∥]Goddard Space Flight Center, NASA, Greenbelt, Maryland 20771, United States

ABSTRACT: Directional photoemission from single Au nanoshells is demonstrated in the low-intensity, multiphoton regime. This directionality is shown to be due to the plasmonic excitation of highly photoemissive, nanometer scale surface regions, which are characterized by correlated momentum mapping, scanning electron microscopy (SEM), and laser polarization-dependence studies. Furthermore, the photoelectron flux from a single nanoshell can be systematically rotated by over 90° in momentum space simply by polarization-controlled coupling to different hot spots. Photoelectron distributions are directly characterized in momentum space via velocity map imaging (VMI) of the two-dimensional transverse (p_x, p_y) momentum components for single nanoshells. For the majority of nanoshells studied, the photoemission is directionally orthogonal to the laser polarization, which implicates nanoscale crevice-shaped "hot spots" clearly observed in the correlated SEM/VMI studies, with the near-field plasmonic nature of these crevices clarified further via finite-element simulations. These results rationalize the large photoemission enhancements observed in previous Au nanoshell studies, but more importantly provide a novel experimental access to directionally tunable electron emission from nanoscale sources. The ability to control photoemission/photocurrent angular distributions at the nanoscale with only modest optical fields indicates a new parameter for optimizing nanoplasmonic system performance and suggests new plasmonic applications such as ultrafast, polarization-controlled photoelectric/photovoltaic switches.

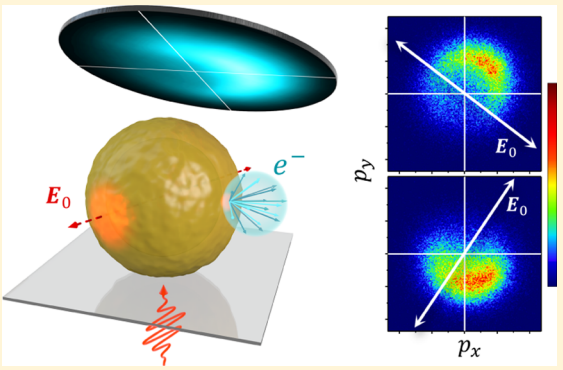

I. INTRODUCTION

Metal nanoparticles with localized surface plasmon resonances (SPRs) are known to act as excellent antennas for concentrating optical fields well below the diffraction limit into deeply sub-wavelength nanoscale volumes. This enables unprecedented control over physical and chemical processes at the nanometer length and femtosecond time scales with the use of readily available tabletop pulsed lasers. High densities of photons, excited charge carriers, and phonons can be generated in nanoscale metal nanoparticle volumes as a consequence of the spatiotemporal localization of the incident resonant light. High photon densities corresponding to high optical intensities are produced around the nanoparticle surface regions where conduction electrons accumulate during SPR oscillations. Electric near-field enhancements in these regions can approach values of $|\mathbf{E}|/|\mathbf{E}_0| \sim 100$, which are utilized in applications such as surface-enhanced Raman spectroscopy (SERS),[1,2] plasmon-assisted photochemistry,[3] and light trapping for novel thin-film solar cells.[4] High densities of hot carriers are produced via nonradiative plasmon decay and may be extracted over/through a Schottky barrier with a surrounding semiconductor as another route toward relatively broadband, thin-film photovoltaic devices such as solar cells and photodetectors.[5−7] Hot carriers can also be ejected into vacuum in photoelectric applications,[8−10] or transferred to chemically bound molecules on nanoparticle surfaces in photocatalytic applications.[3,11−13] The nascent hot carriers thermalize via carrier−carrier scattering (e.g., hot electrons scattering with "cold" Fermi sea electrons) within ∼100 fs and carrier−phonon thermalization takes place within ∼1 ps, heating the nanoparticle lattice.[14] Such nanoparticle heating effects have been exploited for catalyzing surface chemistry,[15] ablating tumors in photothermal cancer therapy,[16] and releasing conjugated biomolecules in targeted drug delivery.[17]

Although the ability to plasmonically couple optical fields into nanoscale volumes is intrinsically useful, additional dynamic control over the plasmonic near-field response offers a particularly important capability for emerging nanoparticle technologies. Near-field control is primarily achieved by manipulating far-field laser parameters such as frequency and polarization to excite different nanoparticle SPR modes.[18−22] Polarization control over the near-electric-field distribution, for

Received: April 10, 2018
Revised: May 31, 2018
Published: June 1, 2018

DOI: 10.1021/acs.jpcc.8b03402
J. Phys. Chem. C 2018, 122, 14805−14813

example, has been demonstrated on sub-picosecond time scales using femtosecond polarization pulse shaping.[23] Laser intensity is an even simpler far-field parameter that can be adjusted to influence the near-field dynamics, by promoting either multiphoton photoemission (MPPE) from metal nanoparticles in the weak-field regime or optical field emission (OFE) in the strong-field regime. Modulation of the laser intensity can therefore serve as a crucial control parameter in photovoltaic and photoelectric applications because the emission mechanism (MPPE vs OFE) can have substantial impact on the spatial, temporal, and momentum distributions of the resulting photocurrents.

Optimal design and control of nanoplasmonic devices requires a detailed understanding of the plasmonic near-field distributions and charge transfer/photoemission behavior as a function of input laser parameters and nanoparticle geometry, material, and environment. In particular, spatially localized, ultrafast, and directionally controllable nanoscale electron sources could lead to a variety of new capabilities and fundamentally new degrees of freedom in the design space for nanoscience and nanotechnology. In the present work, we provide a direct momentum-space demonstration of such level of control, based on exploiting nominally spherical Au nanoshells with few-nanometer surface defect hot spots as polarization-sensitive and directional photoelectric nanoemitters. The focus of this work is a proof-of-principle concept with which to help guide the rational design of more highly controllable and application-specific plasmonic nanosystems. It should be emphasized that the results presented here apply to nano-localized hot spots of all sorts, including at high-curvature surfaces or junctions of nanoparticles/nanostructures,[18,24,25] which can be controlled during synthesis/fabrication. Some particularly novel applications that would take advantage of these far-field-controlled directional photocurrents include site-selective photochemistry,[26,27] nanoplasmonic circuits, or ultrafast photocathodes[28] that are also directionally tunable (e.g., for optical switching of photocurrents on the femtosecond time scale).

A number of studies have demonstrated the implementation of plasmonic nanotips[8,29,30] and nanoparticle arrays[9,24] as ultrafast, directional (even directionally tunable[30,31]), strong-field photocathodes, which may be used as X-ray free electron laser sources[10] and for femtosecond electron microspectroscopy.[8,29] High-energy (>10 eV), highly directional photoelectron distributions have been produced in these applications via ponderomotive or sub-optical-cycle acceleration in strong, evanescent plasmonic fields.[24,32] Complementing these applications, the use of nanoshells and other nanoparticles as ultrafast MPPE nanocathodes offers an excellent source of low-energy photoelectrons (<3 eV), with the correspondingly modest laser intensity demands precluding heating damage that can readily occur in the high-intensity optical field emission (OFE) regime. Photocurrents generated in the perturbative, weak-field regime provide additional unique insights into hot carrier spatial and momentum distributions, which must be considered in real-world photocatalytic[26,27] and photovoltaic[33] applications, particularly with low-peak-intensity (continuous-wave laser) and incoherent (solar, light-emitting diode) light sources. These possibilities are underscored by recent experiments demonstrating readily measurable multiphoton photoemission currents ($>10^4$ e^-/s) from continuous-wave laser excitation of the strong plasmonic hot spots at gold nanostar tips.[34]

Photoemissivity has been spatially mapped at the nanometer scale in previous experiments employing photoemission electron microscopy (PEEM)[18,19] and nanomaterials made via exposure of electron-beam lithographic resists.[35] Surface reactivity and charge transfer efficiency have also been resolved at the nanometer length scale via super-resolution imaging[26] and nanoparticle tagging[27] techniques. Some features of the corresponding momentum-space distributions may be inferred from these spatially resolved studies, but techniques that directly measure photoelectron vector momentum distributions are necessary to understand and control plasmonic photocurrents. Toward this end, two different single-particle momentum mapping systems have been recently developed: (i) a time-of-flight momentum-resolving electron microscope (ToF k-PEEM)[36−38] and (ii) scanning photoelectron imaging microscopy (SPIM).[39] In both cases, nanoparticles are immobilized on a substrate, enabling long-term photoemission investigations and correlated spatial measurements for in-depth investigations of the plasmonic photoemission properties with regard to specific nanoscale geometrical features.

II. EXPERIMENTAL

The SPIM technique utilized here combines the scanning photoemission microscopy/spectroscopy for single-particle characterization[40] with velocity map imaging (VMI) for transverse (p_x, p_y) photoelectron momentum mapping, as described in detail elsewhere.[39] For the present experiments, commercially available Au shell/silica core nanoparticles with lipoic acid ligands (nanoComposix Inc., R_{core} = 60 nm and R_{total} = 82 nm) are spin-coated onto a 10 nm indium tin oxide (ITO) film on a glass coverslip, with the ITO providing charge neutralization following photoemission and >90% visible light transmission in the through-sample excitation scheme indicated in Figure 1a. The substrate area is indexed with a deposited gold grid (30 nm thick with a 2 nm titanium sublayer) for correlated microscopy studies, where the grid is prepared via photomask lithography using a finder grid as the mask (LF-400). Example transmission electron microscopy (TEM) images of the nanoshells deposited on a carbon film are shown in Figure 1b.

Dipolar and quadrupolar scattering properties of the nanoshells are characterized via dark-field microscopy (DFM), with a single-nanoshell scattering spectrum shown in Figure 1c. As described previously,[40] the DFM setup is separate from the SPIM system and consists of white light from a tungsten/halogen lamp focused onto the sample via a dark-field condenser lens. Scattered light is collected via a microscope objective on the opposite side of the sample and imaged onto an electron-multiplying CCD (Princeton Instruments Cascade II) via a spectrometer (Acton SpectraPro 150, 150 grooves/mm grating). The spectrographs from individual nanoparticles are background-corrected and scaled to correct for spectral nonuniformity of the light source, the system transmission function, and the camera sensitivity curve. Unless otherwise indicated, nanoshells in these SPIM experiments are excited with 200 fs pulsed light at $\hbar\omega$ = 1.9 eV (650 nm), which is strongly coupled to the dipolar SPR. The Ti:sapph-pumped optical parametric oscillator can, however, be readily tuned between 515 and 775 nm as necessary.

The polycrystalline gold nanoshells are textured with few-nanometer surface roughness due to the seed-mediated shell growth mechanism,[41] as seen in the transmission electron micrographs in Figure 1b. Although this has minimal effects on

DOI: 10.1021/acs.jpcc.8b03402
J. Phys. Chem. C 2018, 122, 14805−14813

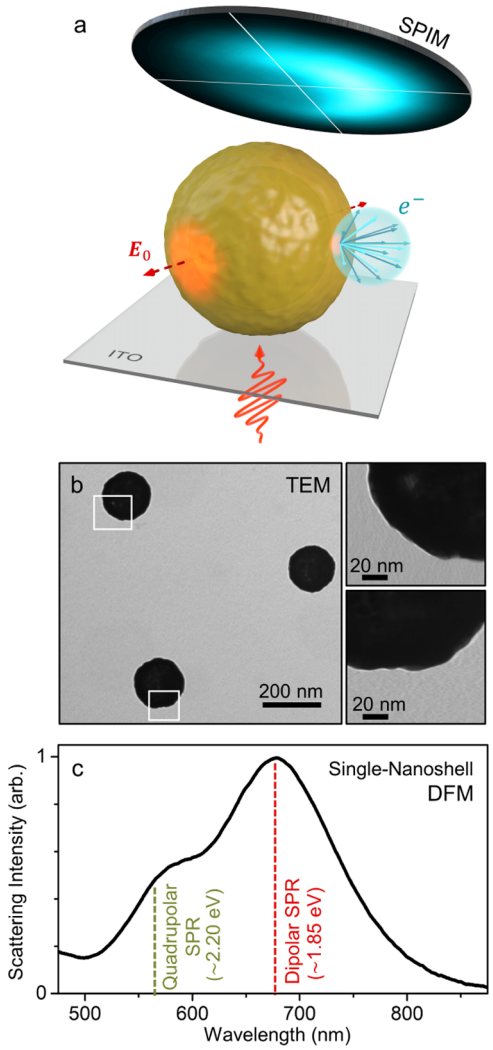

Figure 1. (a) Illustration of the nanoshell excitation scheme in SPIM. (b) Transmission electron micrograph of three nanoshells supported on a carbon film, with high-magnification images demonstrating various gold shell surface roughness features. (c) Representative single-nanoshell scattering spectrum measured via dark-field microscopy (DFM), for a nanoshell supported on an ITO/glass substrate.

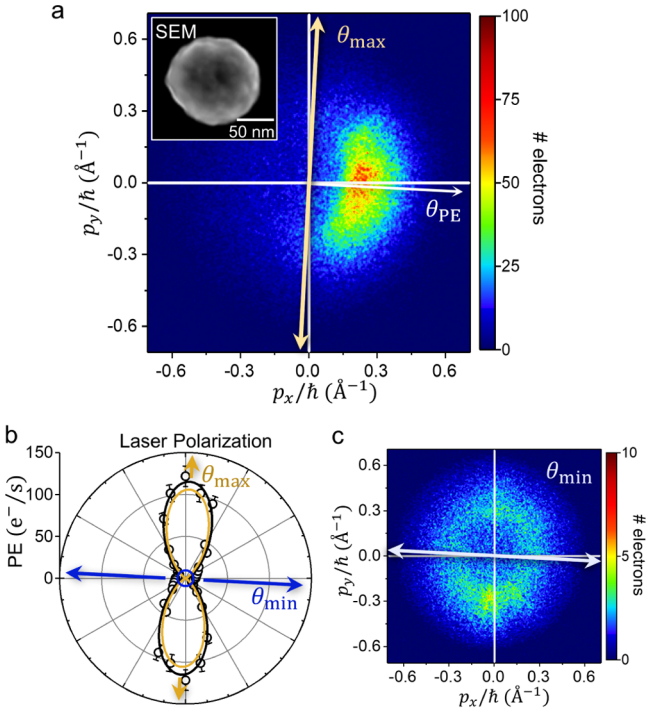

Figure 2. Directional photoemission from a single Au nanoshell, with all measurements taken at $\hbar\omega$ = 1.9 eV on the dipolar SPR. (a) Photoelectron momentum map for a single nanoshell at the maximum photoemission polarization, θ_{max}. (Inset: a correlated SEM image.) (b) Polarization dependence for the same nanoshell, fit to $\cos^{2n}(\theta)$ (with n = 3) for the hot spot plus a constant term for the isotropic nanoshell contribution. (c) Momentum map for the same nanoshell, but now at the minimum photoemission polarization, θ_{min}, which demonstrates a more nearly isotropic photoemission behavior.

the far-field optical properties of Au nanoshells, certain geometries within the surface structure can produce very large plasmonic near-field enhancements ("hot spots") in few-nanometer regions.[42] Surface roughness-based hot spots have been invoked in previous studies to explain the exceptionally high single nanoshell SERS intensities,[43] along with the high photoemissivity and polarization sensitivity of the nominally spherical particles.[44] This few-nanometer hot spot model is corroborated here via correlated SPIM and scanning electron microscopy (SEM) studies. Most importantly, we demonstrate (i) directional MPPE from a nanoscale emission source and (ii) polarization-control over this directionality by coupling to different hot spots.

III. RESULTS

The photoemission rate for a typical Au nanoshell is highly sensitive to the laser polarization even for normal-incidence light, as shown in Figure 2 and explored previously in detail.[44] Because the nanoshells observed via TEM and SEM are nominally spherical, the strong polarization dependence indicates the presence of additional structure such as bumps and/or pits on the surface of the Au shell, which breaks the expected azimuthal symmetry of a supported spherical object. Despite the small individual surface areas of these hot spots relative to the overall nanoshell surface area, it has been shown that plasmonic field enhancements can grow disproportionately relative to a shrinking emitter area with a sharp geometrical feature, thereby enabling even sub-nanometer hot spots to compete with and even dominate the overall photoemissivity.[44] This effect is enhanced even more dramatically in the multiphoton regime, where the photoemission rate is highly nonlinear with respect to the local electric field, scaling as E^{2n} for nPPE. Nanometer-scale surface structure that could potentially produce these effects is evident in the correlated SEM image in the inset of Figure 2a, as well as in the TEM images in Figure 1b. The polarization dependence of the photoemission rate shown in Figure 2b is thus fit by a constant term to account for the underlying isotropic behavior expected for a perfectly smooth nanoshell, which becomes the dominant behavior around the minimum photoemissivity polarization angle, θ_{min}, and a localized hot spot term proportional to $\cos^6(\theta - \theta_{max})$. The latter $2n$th-order cosine term corresponds to the projection of the field along the hot spot axis for a three-photon ($2n = 6$) process. Note that even when polarized along θ_{min}, all of the nanoshells are still orders of magnitude more photoemissive than the ITO substrate.

Photoemission originating from localized hot spots on the nanoshell surface should be leaving the nanoparticle in a well-defined average direction, corresponding approximately to

DOI: 10.1021/acs.jpcc.8b03402
J. Phys. Chem. C 2018, 122, 14805−14813

whichever side of the nanoshell the hot spot is located. The measured photoelectron momentum maps for single nanoshells, as in Figure 2a, confirm the expectation of anisotropic photoemission, which is indeed strongly directional. Contrary to initial expectations, however, a comparison of the momentum map with the polarization dependence for the same nanoshell (Figure 2a,b) reveals that the photoemission is actually strongest in the direction orthogonal to the laser polarization at peak photoemissivity angle, θ_{max}. Moreover, orthogonal photoemission is observed for the majority of nanoshells, with only ∼10% of the nanoshells exhibiting a nominally parallel photoemission relative to the laser polarization at θ_{max} (Figure 3a). Although initially surprising, the

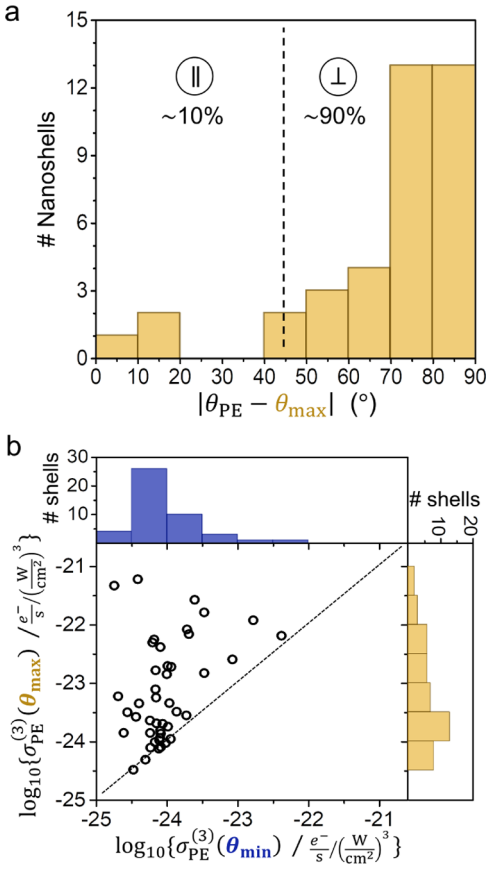

Figure 3. (a) Nanoshell statistics on the average photoemission direction (θ_{PE}) relative to θ_{max}, with θ_{PE} determined via Gaussian fit to radially integrated momentum distributions. (b) Nanoshell photoemissivity statistics at the maximum enhancement polarization, θ_{max}, and minimum enhancement polarization, θ_{min}, for each nanoshell.

orthogonal emission from these hot spots is consistent with a "nanocrevice"-type defect geometry that can readily form between the crystal domains on the polycrystalline shell. At least one of these nanocrevice defects is evident as a dark spot in the micrograph inset in Figure 2a and is also approximately aligned with the peak photoemission direction. As will be shown in further detail via additional correlated SEM-SPIM studies, along with finite-element simulations, these nanocrevice regions can become strong hot spots when the laser polarization is orthogonal to the nanocrevice spatial axis. If the average photoelectron momentum is approximately radially outward from the nanocrevice hot spot region, then the photoemission direction will also be orthogonal to the laser polarization, as observed.

Additional near-field insight is gained by investigating the statistics of nanoshell photoemissivities, $\sigma_{PE}^{(n)}(\theta)$ (where nPPE = $\sigma_{PE}^{(n)}I^n$), over many nanoshells at polarization angles, θ_{max} and θ_{min}. Photoemissivity statistics for 3PPE at $\hbar\omega$ = 1.9 eV are summarized in Figure 3b for 45 individual nanoshells. When combined with correlated momentum maps and SEM images for each nanoshell, these statistics tell a simple story: A given nanoshell surface may contain zero, one, or more nanocrevices, any one of which may become a hot spot when the SPR is driven along the appropriate axis. The maximum nanoshell photoemissivities (at polarization θ_{max}) are spread out over more than 3 orders of magnitude due to very sensitive dependence on the specific crevice geometry and the corresponding near-field enhancement (nPPE ∝ $(|\mathbf{E}|/|\mathbf{E}_0|)^{2n}$). By way of contrast, the minimum photoemissivities are more strongly clustered near the smallest values of $\sigma_{PE}^{(n)}(\theta_{min}) \approx 5 \times 10^{-25} \frac{e^-}{s}/\left(\frac{W}{cm^2}\right)^3$. This indicates that the photoemission at polarization θ_{min} may be reaching the lower limit of the defect-free dipolar SPR enhancement. This picture is corroborated by momentum maps with polarization at $\theta \approx \theta_{min}$, as demonstrated in Figure 2c, which in most cases look quite isotropic despite strong anisotropy/directionality observed with polarization at θ_{max}. It may be noted that even the predominantly isotropic momentum distributions (e.g., Figure 2c) still tend to have a slight preference toward the orthogonal emission relative to the laser polarization, which may be mediated by minor hot spot effects from other small bumps and crevices that cover the nanoshell surface. The total momentum distribution at any laser polarization angle is simply the linear combination of the θ_{min} and θ_{max} distributions, with the latter strongly peaking due to scaling by $\cos^{2n}(\theta - \theta_{max})$.

Before proceeding, we briefly discuss an important experimental protocol for achieving high-quality momentum maps. All of the nanoshell momentum maps initially reveal a predominantly isotropic distribution peaking strongly at zero transverse momentum, which we ascribe to inelastic scattering in the photoemission process due to surface ligands. This occurs regardless of the cleaning method employed before loading the sample into the vacuum system (e.g., UV−ozone exposure, plasma cleaning, and/or solvent rinsing). Such effects have been demonstrated previously for Au nanoshells[39] and attributed to photoelectron scattering from the lipoic acid ligand layer and/or with an adlayer formed during brief (∼10 min) ambient air exposure between sample cleaning and loading into the vacuum chamber. However, as first shown by the El-Sayed group,[45] brief exposure of the nanoshell samples to second harmonic light (here ∼1 GW/cm^2 at 400 nm for ∼1 s, under high vacuum conditions) can break the Au−thiol ligand bonds. In our VMI apparatus, this appears to eliminate the isotropically scattered photoemission contribution near zero energy, thereby revealing the anisotropic photoemission distributions of primary fundamental interest. Most importantly, this procedure only eliminates the inelastically scattered central peak near zero energy and has no effect on the underlying photoemission behavior, with the same directionality of the photoemission observed before and after 400 nm light exposure. Furthermore, this in vacuo laser cleaning is highly reproducible, yielding qualitatively identical results for every nanoshell studied. It can also be performed quickly and efficiently using the scanning stage to clean dozens of

DOI: 10.1021/acs.jpcc.8b03402
J. Phys. Chem. C 2018, 122, 14805−14813

nanoshells in a target area before study. No additional changes are observed in the photoelectron momentum distributions for longer exposures or higher intensities, indicating that photoelectron scattering with the lipoic acid ligands and/or other adlayer effects have been largely eliminated, presumably by ligand/adlayer removal. Finally, we have only observed this cleaning effect for 3.1 eV (400 nm) or higher-energy photons, with no significant effect evident even with higher intensities of the most energetic optical parametric oscillator output (~2.3 eV photons). In their previous study of ligand removal due to Au−S bond cleavage upon exposure to 400 nm light, Jain et al. attributed the phenomenon to hot electron energy transfer into the Au−S bond dissociation coordinate.[45]

To verify that all directional photoemission observed in these experiments is due to hot spot MPPE enhancement rather than OFE and/or ponderomotive acceleration following emission, photoelectron transverse kinetic energy distributions have been recorded at multiple different laser intensities and frequencies. The results are presented in Figure 4 for a single nanoshell, in this case, one displaying the less typical behavior of peak photoemission (with polarization at θ_{max}) parallel to the laser polarization axis (Figure 4a). Even for these uncommon parallel emitters, the intensity- and frequency-dependent behavior demonstrated in Figure 4 is completely consistent with the more commonly observed perpendicular emitters. Specifically, as the intensity is increased in Figure 4b in uniform steps of 0.2 GW/cm^2 at $\hbar\omega$ = 1.90 eV, the total photoemission signal increases as I^3 (as expected for 3PPE), but the transverse kinetic energy distributions remain largely unchanged. This strongly supports a three-photon photoemission (3PPE) process. Conversely, although ponderomotive acceleration could in principle be taking place following MPPE in strong hot spot evanescent fields, one would expect the kinetic energy cutoff to increase approximately linearly with laser intensity,[46] whereas no such change is observed in the kinetic energy spectra over a 5-fold change in intensity. Furthermore, the Fermi edge drop-off around 1.5 eV kinetic energy corresponds to the expected value for 3PPE: $3\hbar\omega - \phi = 5.7 - 4.2$ eV = 1.5 eV, in which the supported nanoshell work function of ~4.2 eV was also measured previously.[39] Thus, we can be quite certain of these experiments being in the fully perturbative 3PPE regime.

For gain further insight into the photoemission dynamics from nanoshell hot spots, transverse kinetic energy spectra have been measured as a function of laser photon energy, shown in Figure 4c. These results are perfectly consistent with the MPPE mechanism, with the Fermi edge expanding outward by $\sim\Delta(n\hbar\omega)$ with increasing photon energy and with a clear transition from the 3PPE regime to the 2PPE occurring between $\hbar\omega$ = 1.90 and 2.20 eV. This sharp transition is quite strikingly revealed in the inset of Figure 4c, which summarizes the power-law fits to intensity-dependence studies at a series of laser photon energies (nPPE $\propto I^n$) and, as expected, displays a precipitous sigmoidal shift in behavior between n = 3 and 2. In contrast, none of this behavior is expected in an OFE process, nor in a thermionic process.

As a final confirmation of the multiphoton process, the Keldysh parameter (γ), interpreted simply as the ratio of the optical frequency to the tunneling frequency, provides a convenient single-parameter indicator for MPPE ($\gamma > 1$) versus OFE ($\gamma < 1$).[47] At the highest peak input intensities at the sample of 1 GW/cm^2 ($E_0 \approx 0.1$ V/nm), for a measured nanoshell work function around 4.2 eV and assuming a large

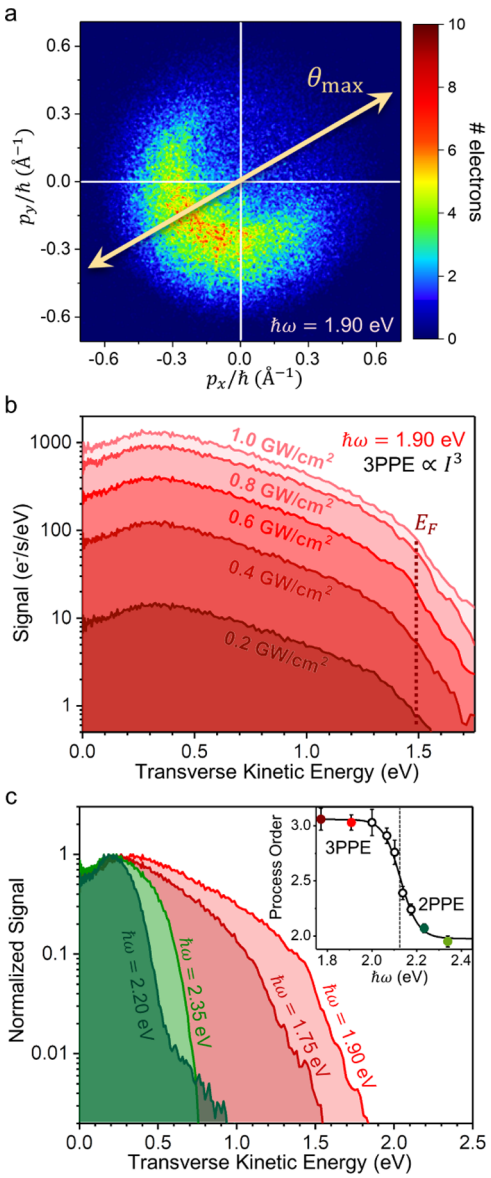

Figure 4. Confirmation that all photoemission takes place in the perturbative multiphoton regime. (a) Momentum map for a nanoshell/hot spot exhibiting a nearly parallel emission (but the demonstrated behavior is equally valid for the much more common orthogonal emitters). (b) Angle-integrated transverse kinetic energy spectra as a function of peak pulse intensity. The dashed line represents the kinetic energy of electrons originating from around the Fermi level within the gold. (c) Angle-integrated transverse kinetic energy spectra for different incident photon energies. (Inset: Summary of laser intensity-dependence measurements, with the process order determined via power-law fit, where nPPE $\propto I^n$). The tail evident in the $\hbar\omega$ = 2.20 eV 2PPE distribution is due to a remaining 3PPE contribution, due to proximity to the 2PPE−3PPE cross-over frequency ($\hbar\omega$ = 2.15 eV).

hot spot E-field enhancement of 50 at $\hbar\omega$ = 1.90 eV, the Keldysh parameter is $\gamma = \sqrt{\phi/(2U_p)} = 4.6$, with a ponderomotive energy $U_p = e^2E^2/(4m_e\omega^2) \approx 0.1$ eV. These values indicate that photoemission is occurring in the multiphoton regime with minimal post-emission ponderomotive acceleration, even under the most extreme hot spot conditions expected in these experiments. In combination with the laser intensity and frequency studies discussed above, these

DOI: 10.1021/acs.jpcc.8b03402
J. Phys. Chem. C 2018, 122, 14805−14813

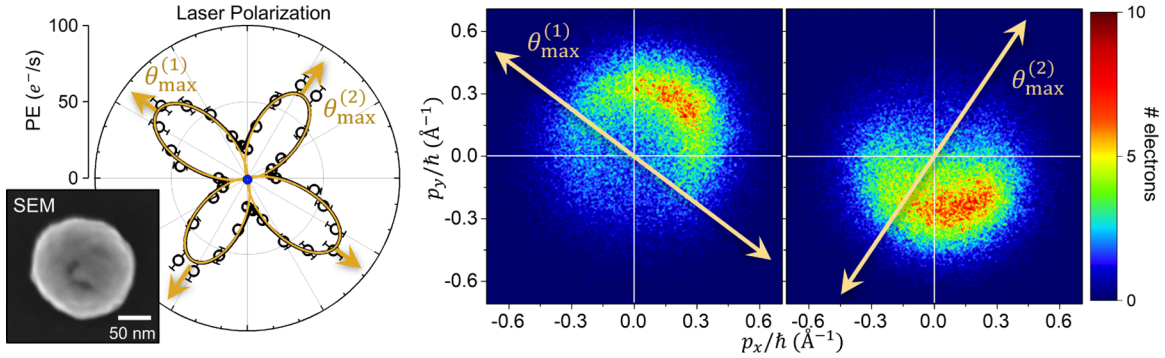

Figure 5. Polarization-controlled directional 3PPE from a single nanoshell with multiple hot spots of nearly identical photoemissivity, excited at $\hbar\omega$ = 1.9 eV.

calculations confirm unambiguously that the directional photoemission occurs from MPPE processes, arising from the specific geometries and nano-localized nature of the nanoshell defect hot spots rather than strong-field acceleration effects.

Unlike surface- or nanotip-based photocathodes, which impose directionality via the macroscopic geometry, the directionality of photoemission from nanoparticles is potentially more subtle, versatile, and tunable in nanoshells by choice of different SPR hot spots. This tunability is clearly demonstrated on a nanoshell that happens to have two hot spots with different θ_{max} but nearly equal photoemission efficiencies, as shown in Figure 5. For such a system, rotation of the laser polarization between $\theta^{(1)}_{max}$ and $\theta^{(2)}_{max}$ also rotates the photoemission direction by a nearly equivalent angle (in the present case, approximately 90°). This illustrates the basic concept for an optically controlled photocurrent switch, which could be operated on the femtosecond time scales via ultrafast polarization control. Although the occurrence of nearly equivalent hot spots is not common in these nanoshells due to the variability of defect geometries and the strong $(|\mathbf{E}|/|\mathbf{E}_0|)^6$ photoemission sensitivity to electric field, this photoemission switching behavior is in fact observed for many nanoshells, just with different hot spot photoemissivities. More importantly, this provides a proof-of-concept for how nanoparticles/nanostructures might be specifically synthesized/fabricated for a near-field control of photoemission properties. For example, nanoparticles such as nanostars[18] or tailored nanolithographic structures[23] could take advantage of this effect in a far more controlled manner, with multiple inherently strong hot spots occurring near the sharply pointed tips.

Recalling (Figure 3a) that the majority of the nanoshell hot spots exhibit a maximum photoemission orthogonal to the laser polarization direction, we can exploit a combination of SEM and finite-element modeling to explore which shell topologies might be most likely to produce this behavior. Correlated SEM and VMI images of 45 sample nanoshells reveal a common crevice-type structure corresponding to dark spots on the nanoshell surface (or light spots in TEM), as highlighted in Figure 6. Indeed, the peak VMI photoemission direction is correlated with one of these crevices in approximately 40% of the nanoshells studied. This 40% correlation is entirely reasonable because approximately half of the nanoshells would be expected to have hot spots in the lower hemisphere (not visible in the SEM images), whereas some will have crevices on the sides of the nanoshells that are less evident in the electron beam imaging. It is thus likely that the observed crevices (or subfeatures therein) represent a common geometry

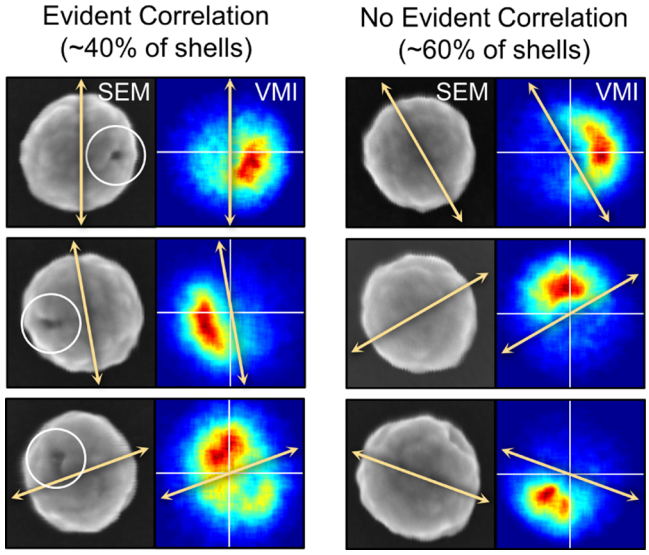

Figure 6. Example SEM and VMI images on single nanoshells that show either (left panel) a clear correlation or (right panel) no correlation between the directional photoemission and a nanoshell surface feature.

for a highly photoemissive hot spot.[42] Previous studies have indeed highlighted the nanocrevice geometry as a probable candidate responsible for the extra strong field enhancements observed with nanoshells and rough metal surfaces.[42,44,48] It is worth noting that the crevice location on the nanoshell in Figure 5 is not aligned with the photoemission directionality. This falls into the category of nanoshells that do not display clear directional correlations (see other examples in Figure 6), possibly due to crevices hidden in the lower hemisphere. It is also possible that the photoemission direction is not perfectly aligned with a crevice evident in SEM/TEM due to a more complex hot spot geometry. Toward this end, we are pursuing improved synthetic or photolithographic methods for preparing nanoplasmonic structures with well-engineered hot spots as an interesting direction with which to establish these statistical correlations more rigorously and to thereby provide a greater angular control over photoemission directionality.

IV. DISCUSSION

Different nanometer-scale features could lead to strong hot spots and photoemission enhancements even within the constraints imposed by these correlated SEM/VMI studies. To help elucidate these features further, we have therefore

DOI: 10.1021/acs.jpcc.8b03402
J. Phys. Chem. C 2018, 122, 14805−14813

utilized the finite-element analysis (FEA) to explore the electric near-field enhancements for a given nanocrevice defect geometry embedded into the side of a nanoshell. Sample surface field enhancements are calculated in COMSOL 5.3 and presented in Figure 7a,c, where it can be seen that the crevice

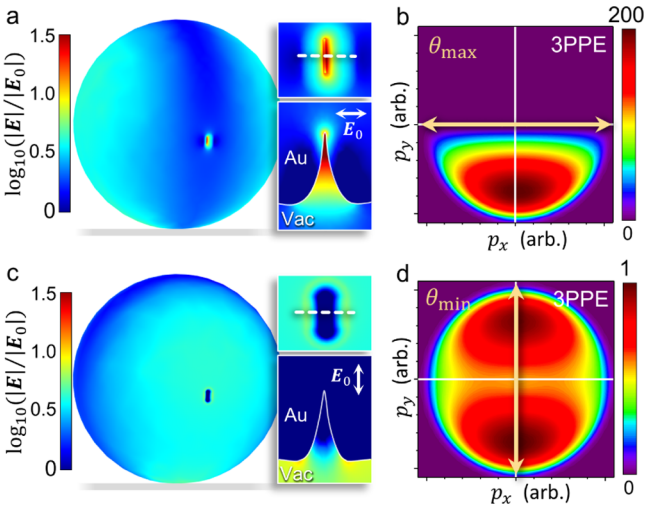

Figure 7. Finite-element simulations (a, c) of the near electric field distribution and corresponding model velocity map images (b, d) for the calculated electron flux around a nanoshell with a single nanocrevice are shown for orthogonal (a, b) and parallel (c, d) polarization of the laser relative to the hot spot radial direction. See text for model details.

becomes a strongly enhanced hot spot when the laser is polarized orthogonal to the crevice radial vector (Figure 7a), whereas the hot spot exhibits negligible field enhancement for parallel polarization. If we consider a photoemission model that assumes a local photoemissivity dependent on surface E-field enhancement to the 2*n*th-order, then a 10-fold E-field hot spot enhancement for this sample geometry would correspond to a peak 3PPE enhancement (per unit surface area) of ~10^6. Using this model as a simple starting point, we integrate the calculated E-field (raised to the appropriate $n = 6$ power for 3PPE) over the entire nanoshell surface. This already predicts an overall 200-fold enhancement of hot spot photoemission for perpendicular (θ_{max}) vs parallel (θ_{min}) polarization.

Furthermore, the FEA near-field distributions for orthogonal laser polarization in Figure 7a suggest a very simple physical mechanism for the field enhancements: the crevice behaves like a nanogap—or a nanoscale capacitor—with the strongest enhancement occurring at the parallel, closely spaced walls near the crevice apex. To avoid unphysically small feature sizes in the model that could lead to singularities in the field enhancements, the smallest radius of curvature in these simulations is limited to the radius of a single gold atom (~1.7 Å). Variation in the crevice parameters (e.g., depth and curvature) changes the exact values of field enhancement, but no essential features of the hot spot behavior. Although such predictions will depend on the precise characterization of the nanocrevice geometry, these model FEA results already rationalize the many orders of magnitude dynamic range in photoemissivity enhancements observed experimentally (see Figure 3b).

We can attempt to model the hot spot photoelectron momentum distributions by performing a surface integral of the flux contributions from each nanoshell surface area element. As mentioned above, the photoelectron fluxes are taken to be proportional to the surface E-field enhancement raised to the $2n = 6$ power appropriate to 3PPE, with these enhancements determined via the previously discussed FEA results and mapped as a fine, uniform mesh over the entire nanoshell surface. The momentum distribution from each surface area element is based on a ballistic three-step model,[49] as discussed recently in the context of SPIM momentum mapping experiments.[39] Briefly summarized, a Fermi–Dirac speed distribution is assumed inside the nanoshell, with the emitted photoelectron distribution scaled by a $p\cos\theta$ Jacobian transformation from internal to external coordinates, whereby velocity components are treated by the usual conservation of energy (i.e., work function) and parallel momentum at the surface potential barrier. The emission from each nanoshell surface area element is taken to be centered relative to the radial vector (i.e., outward from the center of the nanoshell), which invokes the simple intuitive idea that, once the complicated near-field collision dynamics within the defect have played out, the photoelectrons will be ejected approximately radially outward from the hot spot region. Such near-field dynamics include diffusion in the gold before emission and the reabsorption or multiple scattering events that may occur for many photoelectron trajectories due to nonconvex crevice geometries.

The resulting p_z-integrated (p_x, p_y) momentum maps predicted from this simple physical model are shown in Figure 7b,d for a laser polarization orthogonal ($\theta \approx \theta_{max}$) and parallel ($\theta \approx \theta_{min}$) to the nanocrevice axis, respectively. The results for orthogonal polarization in Figure 7b reproduce the essential qualitative behavior observed in the experimental distributions, namely, strong directional photoemission (i) orthogonal to the laser polarization axis and (ii) radially away from the crevice geometry. In contrast, for parallel polarization at θ_{min}, the crevice exhibits E fields unenhanced by any plasmonic effects, resulting in a much weaker (200× less) photoemission characterized by a dipolar SPR near-field distribution and with the peak emission aligned with the laser polarization axis. Interestingly, however, the experimental photoelectron momentum maps at $\theta \approx \theta_{min}$ are rarely perfectly aligned parallel to the laser polarization, typically appearing azimuthally isotropic or even having a slight tendency toward orthogonal emission (e.g., Figure 2c). This suggests that the actual spherical-shell dipolar behavior demonstrated in the idealized calculations of Figure 7d may still be influenced by photoemission contributions from additional sources of crevice-like surface roughness that tend to favor orthogonal rather than parallel emission.

V. SUMMARY AND CONCLUSIONS

In summary, transverse (p_x, p_y) photoelectron momentum maps of single Au nanoshells have been explored to reveal highly directional photoemission distributions in the weak-field MPPE regime. Combined evidence from momentum mapping, laser polarization studies, nanoshell photoemissivity statistics, and SEM imaging suggests that small crevices in the nanoshell surface play an important role, leading to directional emission and corroborating previous work revealing the presence of nanoscale hot spots on Au nanoshell surfaces.[42−44] For the great majority (90%) of the nanoshells, the photoemission direction is orthogonal to the peak laser polarization axis, indicating that the hot spots are due to the nanocrevice-type roughness seen under scanning electron microscopy and

DOI: 10.1021/acs.jpcc.8b03402
J. Phys. Chem. C 2018, 122, 14805−14813

simulated via finite-element analysis. Polarization control over the near-field electron photoemission behavior has been demonstrated for a single nanoshell with dual hot spots, providing a proof of concept for the engineering of plasmonic nanostructures with selective directional control of photoemission via laser polarization, which can be rotated on ultrafast time scales. Though not specifically demonstrated here, directional control could also be achieved by addressing different hot spots via laser frequency tuning. It is our hope that the MPPE behavior demonstrated in these studies for single nanoshells provides new insights into and simple guiding principles for engineering novel optical and electronic near-field behaviors in future nanoplasmonic applications.

AUTHOR INFORMATION

Corresponding Author

*E-mail: djn@jila.colorado.edu.

ORCID

David J. Nesbitt: 0000-0001-5365-1120

Author Contributions

The manuscript was written through contributions from all the authors, with all the authors indicating approval of the final version.

Notes

The authors declare no competing financial interest.

ACKNOWLEDGMENTS

This work has been supported by the Air Force Office of Scientific Research (FA9550-15-1-0090), with additional funds for vacuum equipment and lasers provided by the National Science Foundation (CHE 1266416, PHYS 1125844).

REFERENCES

(1) Stiles, P. L.; Dieringer, J. A.; Shah, N. C.; Van Duyne, R. P. Surface-Enhanced Raman Spectroscopy. *Annu. Rev. Anal. Chem.* **2008**, *1*, 601−626.

(2) Gruenke, N. L.; Cardinal, M. F.; McAnally, M. O.; Frontiera, R. R.; Schatz, G. C.; Van Duyne, R. P. Ultrafast and Nonlinear Surface-Enhanced Raman Spectroscopy. *Chem. Soc. Rev.* **2016**, *45*, 2263−2290.

(3) Baffou, G.; Quidant, R. Nanoplasmonics for Chemistry. *Chem. Soc. Rev.* **2014**, *43*, 3898−3907.

(4) Spinelli, P.; Ferry, V. E.; van de Groep, J.; van Lare, M.; Verschuuren, M. A.; Schropp, R. E. I.; Atwater, H. A.; Polman, A. Plasmonic Light Trapping in Thin-Film Si Solar Cells. *J. Opt.* **2012**, *14*, No. 024002.

(5) Mubeen, S.; Hernandez-Sosa, G.; Moses, D.; Lee, J.; Moskovits, M. Plasmonic Photosensitization of a Wide Band Gap Semiconductor: Converting Plasmons to Charge Carriers. *Nano Lett.* **2011**, *11*, 5548−5552.

(6) Clavero, C. Plasmon-Induced Hot-Electron Generation at Nanoparticle/Metal-Oxide Interfaces for Photovoltaic and Photocatalytic Devices. *Nat. Photonics* **2014**, *8*, 95−103.

(7) Brongersma, M. L.; Halas, N. J.; Nordlander, P. Plasmon-Induced Hot Carrier Science and Technology. *Nat. Nanotechnol.* **2015**, *10*, 25−34.

(8) Müller, M.; Kravtsov, V.; Paarmann, A.; Raschke, M. B.; Ernstorfer, R. Nanofocused Plasmon-Driven Sub-10 fs Electron Point Source. *ACS Photonics* **2016**, *3*, 611−619.

(9) Hobbs, R. G.; Yang, Y.; Fallahi, A.; Keathley, P. D.; De Leo, E.; Kärtner, F. X.; Graves, W. S.; Berggren, K. K. High-Yield, Ultrafast, Surface Plasmon-Enhanced, Au Nanorod Optical Field Electron Emitter Arrays. *ACS Nano* **2014**, *8*, 11474−11482.

(10) Graves, W. S.; Kärtner, F. X.; Moncton, D. E.; Piot, P. Intense Superradiant X Rays from a Compact Source Using a Nanocathode Array and Emittance Exchange. *Phys. Rev. Lett.* **2012**, *108*, No. 263904.

(11) Mukherjee, S.; Libisch, F.; Large, N.; Neumann, O.; Brown, L. V.; Cheng, J.; Lassiter, J. B.; Carter, E. A.; Nordlander, P.; Halas, N. J. Hot Electrons Do the Impossible: Plasmon-Induced Dissociation of H_2 on Au. *Nano Lett.* **2013**, *13*, 240−247.

(12) Boerigter, C.; Aslam, U.; Linic, S. Mechanism of Charge Transfer from Plasmonic Nanostructures to Chemically Attached Materials. *ACS Nano* **2016**, *10*, 6108−6115.

(13) Brandt, N. C.; Keller, E. L.; Frontiera, R. R. Ultrafast Surface-Enhanced Raman Probing of the Role of Hot Electrons in Plasmon-Driven Chemistry. *J. Phys. Chem. Lett.* **2016**, *7*, 3179−3185.

(14) Hartland, G. V. Optical Studies of Dynamics in Noble Metal Nanostructures. *Chem. Rev.* **2011**, *111*, 3858−3887.

(15) Linic, S.; Aslam, U.; Boerigter, C.; Morabito, M. Photochemical Transformations on Plasmonic Metal Nanoparticles. *Nat. Mater.* **2015**, *14*, 567−576.

(16) Dreaden, E. C.; Alkilany, A. M.; Huang, X. H.; Murphy, C. J.; El-Sayed, M. A. The Golden Age: Gold Nanoparticles for Biomedicine. *Chem. Soc. Rev.* **2012**, *41*, 2740−2779.

(17) Wijaya, A.; Schaffer, S. B.; Pallares, I. G.; Hamad-Schifferli, K. Selective Release of Multiple DNA Oligonucleotides from Gold Nanorods. *ACS Nano* **2009**, *3*, 80−86.

(18) Hrelescu, C.; Sau, T. K.; Rogach, A. L.; Jackel, F.; Laurent, G.; Douillard, L.; Charra, F. Selective Excitation of Individual Plasmonic Hotspots at the Tips of Single Gold Nanostars. *Nano Lett.* **2011**, *11*, 402−407.

(19) Awada, C.; Popescu, T.; Douillard, L.; Charra, F.; Perron, A.; Yockell-Lelievre, H.; Baudrion, A. L.; Adam, P. M.; Bachelot, R. Selective Excitation of Plasmon Resonances of Single Au Triangles by Polarization-Dependent Light Excitation. *J. Phys. Chem. C* **2012**, *116*, 14591−14598.

(20) Melchior, P.; Bayer, D.; Schneider, C.; Fischer, A.; Rohmer, M.; Pfeiffer, W.; Aeschlimann, M. Optical Near-Field Interference in the Excitation of a Bowtie Nanoantenna. *Phys. Rev. B* **2011**, *83*, No. 235407.

(21) Grubisic, A.; Ringe, E.; Cobley, C. M.; Xia, Y. N.; Marks, L. D.; Van Duyne, R. P.; Nesbitt, D. J. Plasmonic near-Electric Field Enhancement Effects in Ultrafast Photoelectron Emission: Correlated Spatial and Laser Polarization Microscopy Studies of Individual Ag Nanocubes. *Nano Lett.* **2012**, *12*, 4823−4829.

(22) Baker, T. A.; Grubisic, A.; Nesbitt, D. J. Plasmon Mediated Multiphoton Photoemission Microscopy of Au Nanoholes and Nanohole Dimers. *J. Phys. Chem. C* **2014**, *118*, 6959−6971.

(23) Aeschlimann, M.; Bauer, M.; Bayer, D.; Brixner, T.; Cunovic, S.; Dimler, F.; Fischer, A.; Pfeiffer, W.; Rohmer, M.; Schneider, C.; et al. Spatiotemporal Control of Nanooptical Excitations. *Proc. Natl. Acad. Sci. U.S.A.* **2010**, *107*, 5329−5333.

(24) Dombi, P.; Horl, A.; Racz, P.; Marton, I.; Trugler, A.; Krenn, J. R.; Hohenester, U. Ultrafast Strong-Field Photoemission from Plasmonic Nanoparticles. *Nano Lett.* **2013**, *13*, 674−678.

(25) Henry, A. I.; Bingham, J. M.; Ringe, E.; Marks, L. D.; Schatz, G. C.; Van Duyne, R. P. Correlated Structure and Optical Property Studies of Plasmonic Nanoparticles. *J. Phys. Chem. C* **2011**, *115*, 9291−9305.

(26) Sambur, J. B.; Chen, T. Y.; Choudhary, E.; Chen, G. Q.; Nissen, E. J.; Thomas, E. M.; Zou, N. M.; Chen, P. Sub-Particle Reaction and Photocurrent Mapping to Optimize Catalyst-Modified Photoanodes. *Nature* **2016**, *530*, 77−93.

(27) Cortés, E.; Xie, W.; Cambiasso, J.; Jermyn, A. S.; Sundararaman, R.; Narang, P.; Schlucker, S.; Maier, S. A. Plasmonic Hot Electron Transport Drives Nano-Localized Chemistry. *Nat. Commun.* **2017**, *8*, No. 14880.

(28) Ye, H.; Trippel, S.; Di Fraia, M.; Fallahi, A.; Mücke, O. D.; Kärtner, F. X.; Küpper, J. Velocity-Map Imaging for Emittance Characterization of Multiphoton Electron Emission from a Gold Surface. *Phys. Rev. Appl.* **2018**, *9*, No. 044018.

(29) Schröder, B.; Sivis, M.; Bormann, R.; Schafer, S.; Ropers, C. An Ultrafast Nanotip Electron Gun Triggered by Grating-Coupled Surface Plasmons. *Appl. Phys. Lett.* **2015**, *107*, No. 231105.

DOI: 10.1021/acs.jpcc.8b03402
J. Phys. Chem. C 2018, 122, 14805−14813

(30) Park, D. J.; Piglosiewicz, B.; Schmidt, S.; Kollmann, H.; Mascheck, M.; Lienau, C. Strong Field Acceleration and Steering of Ultrafast Electron Pulses from a Sharp Metallic Nanotip. *Phys. Rev. Lett.* **2012**, *109*, No. 244803.
(31) Yanagisawa, H.; Hafner, C.; Dona, P.; Klockner, M.; Leuenberger, D.; Greber, T.; Osterwalder, J.; Hengsberger, M. Laser-Induced Field Emission from a Tungsten Tip: Optical Control of Emission Sites and the Emission Process. *Phys. Rev. B* **2010**, *81*, No. 115429.
(32) Herink, G.; Solli, D. R.; Gulde, M.; Ropers, C. Field-Driven Photoemission from Nanostructures Quenches the Quiver Motion. *Nature* **2012**, *483*, 190−193.
(33) Knight, M. W.; Wang, Y. M.; Urban, A. S.; Sobhani, A.; Zheng, B. Y.; Nordlander, P.; Halas, N. J. Embedding Plasmonic Nanostructure Diodes Enhances Hot Electron Emission. *Nano Lett.* **2013**, *13*, 1687−1692.
(34) Sivis, M.; Pazos-Perez, N.; Yu, R.; Alvarez-Puebla, R.; de Abajo, F. J. G.; Ropers, C. Continuous-Wave Multiphoton Photoemission from Plasmonic Nanostars. *Commun. Phys.* **2018**, *1*, No. 13.
(35) Hobbs, R. G.; Putnam, W. P.; Fallahi, A.; Yang, Y. J.; Kärtner, F. X.; Berggren, K. K. Mapping Photoemission and Hot-Electron Emission from Plasmonic Nanoantennas. *Nano Lett.* **2017**, *17*, 6069−6076.
(36) Lehr, M.; Foerster, B.; Schmitt, M.; Kruger, K.; Sonnichsen, C.; Schonhense, G.; Elmers, H. J. Momentum Distribution of Electrons Emitted from Resonantly Excited Individual Gold Nanorods. *Nano Lett.* **2017**, *17*, 6606−6612.
(37) Schönhense, G.; Medjanik, K.; Chernov, S.; Kutnyakhov, D.; Fedchenko, O.; Ellguth, M.; Vasilyev, D.; Zaporozhchenko-Zymakova, A.; Panzer, D.; Oelsner, A.; et al. Spin-Filtered Time-of-Flight K-Space Microscopy of Ir - Towards the "Complete" Photoemission Experiment. *Ultramicroscopy* **2017**, *183*, 19−29.
(38) Schönhense, G.; Medjanik, K.; Elmers, H. J. Space-, Time- and Spin-Resolved Photoemission. *J. Electron Spectrosc. Relat. Phenom.* **2015**, *200*, 94−118.
(39) Pettine, J.; Grubisic, A.; Nesbitt, D. J. Angle- and Momentum-Resolved Photoelectron Velocity Map Imaging Studies of Thin Au Film and Single Supported Au Nanoshells. *J. Phys. Chem. C* **2018**, *122*, 3970−3984.
(40) Grubisic, A.; Schweikhard, V.; Baker, T. A.; Nesbitt, D. J. Coherent Multiphoton Photoelectron Emission from Single Au Nanorods: The Critical Role of Plasmonic Electric Near-Field Enhancement. *ACS Nano* **2013**, *7*, 87−99.
(41) Oldenburg, S. J.; Averitt, R. D.; Westcott, S. L.; Halas, N. J. Nanoengineering of Optical Resonances. *Chem. Phys. Lett.* **1998**, *288*, 243−247.
(42) Hao, E.; Li, S. Y.; Bailey, R. C.; Zou, S. L.; Schatz, G. C.; Hupp, J. T. Optical Properties of Metal Nanoshells. *J. Phys. Chem. B* **2004**, *108*, 1224−1229.
(43) Talley, C. E.; Jackson, J. B.; Oubre, C.; Grady, N. K.; Hollars, C. W.; Lane, S. M.; Huser, T. R.; Nordlander, P.; Halas, N. J. Surface-Enhanced Raman Scattering from Individual Au Nanoparticles and Nanoparticle Dimer Substrates. *Nano Lett.* **2005**, *5*, 1569−1574.
(44) Grubisic, A.; Mukherjee, S.; Halas, N.; Nesbitt, D. J. Anomalously Strong Electric Near-Field Enhancements at Defect Sites on Au Nanoshells Observed by Ultrafast Scanning Photoemission Imaging Microscopy. *J. Phys. Chem. C* **2013**, *117*, 22545−22559.
(45) Jain, P. K.; Qian, W.; El-Sayed, M. A. Ultrafast Cooling of Photoexcited Electrons in Gold Nanoparticle-Thiolated DNA Conjugates Involves the Dissociation of the Gold-Thiol Bond. *J. Am. Chem. Soc.* **2006**, *128*, 2426−2433.
(46) Kupersztych, J.; Monchicourt, P.; Raynaud, M. Ponderomotive Acceleration of Photoelectrons in Surface-Plasmon-Assisted Multiphoton Photoelectric Emission. *Phys. Rev. Lett.* **2001**, *86*, 5180−5183.
(47) Keldysh, L. V. Ionization in Field of a Strong Electromagnetic Wave. *Sov. Phys. JETP-USSR* **1965**, *20*, 1307−1314.
(48) García-Vidal, F. J.; Pendry, J. B. Collective Theory for Surface Enhanced Raman Scattering. *Phys. Rev. Lett.* **1996**, *77*, 1163−1166.
(49) Berglund, C. N.; Spicer, W. E. Photoemission Studies of Copper and Silver: Theory. *Phys. Rev. A* **1964**, *136*, A1030−A1044.

DOI: 10.1021/acs.jpcc.8b03402
J. Phys. Chem. C 2018, 122, 14805−14813